

# Nanodiamond interferometry meets quantum gravity

Andreas Albrecht,<sup>1,2</sup> Alex Retzker,<sup>3</sup> and Martin B Plenio<sup>1,2</sup>

<sup>1</sup>*Institut für Theoretische Physik, Albert-Einstein-Allee 11, Universität Ulm, 89069 Ulm, Germany*

<sup>2</sup>*Center for Integrated Quantum Science and Technology, Universität Ulm, 89069 Ulm, Germany*

<sup>3</sup>*Racah Institute of Physics, The Hebrew University of Jerusalem, Jerusalem 91904, Israel*

Interferometry with massive particles may have the potential to explore the limitations of standard quantum mechanics in particular where it concerns its boundary with general relativity and the yet to be developed theory of quantum gravity. This development is hindered considerably by the lack of experimental evidence and testable predictions. Analyzing effects that appear to be common to many of such theories, such as a modification of the energy dispersion and of the canonical commutation relation within the standard framework of quantum mechanics, has been proposed as a possible way forward. Here we analyze in some detail the impact of a modified energy-momentum dispersion in a Ramsey-Bordé setup and provide achievable bounds of these correcting terms when operating such an interferometer with nanodiamonds. Thus, taking thermal and gravitational disturbances into account will show that without specific prerequisites, quantum gravity modifications may in general be suppressed requiring a revision of previously estimated bounds. As a possible solution we propose a stable setup that is rather insensitive to these effects. Finally, we address the problems of decoherence and pulse errors in such setups and discuss the scalings and advantages with increasing particle mass.

A framework, unifying classical general relativity with quantum mechanics, remains a crucial scientific challenge to date. As incompatibilities hinder the straightforward inclusion of gravity into the standard framework of quantum field theory, the development of a new theory, the quantum gravity, seems essential. Spacetime quantization is a natural ingredient of such a theory stemming from its dynamical nature in general relativity. This has led to the notion of minimal length- and maximal energy scales [1, 2], commonly ascribed to the Planck-scales: The Planck-length  $l_p$  as the length where the Compton radius of quantum mechanics meets the Schwarzschild equivalent of gravitation  $l_p = \sqrt{G\hbar/(c^3)} \simeq 1.6 \cdot 10^{-35} m$  and the Planck mass  $M_p = \hbar/(cL_p) = \sqrt{\hbar c/G} \simeq 2.1 \cdot 10^{-8} kg$ . More abstract, these scales arise in a combination of three fundamental constants, thereby forming new quantities that may or may not be of fundamental importance in nature. This minimal lengthscale plays a crucial role in quantum gravity theories [1] as string theory [3, 4], loop quantum gravity [5], doubly special relativity [6, 7] and in the field of black hole physics [8]. The complete frameworks however are rather complex and incomplete in their physical interpretation. It has therefore been proposed to test common impacts of a spacetime quantization on standard quantum mechanics instead, such as the modification of the energy dispersion relation [9] or the change of quantum mechanical commutator relations [2, 10–12]. Incorporating such ‘universal’ effects into existing frameworks inspired the proposal of numerous verification experiments both in the relativistic and non-relativistic regime. This has led to bounds on the magnitude of the anticipated fundamental scales, though, due to the smallness of the effects, an existence verification is still pending. In particular tests have been proposed within the framework of quantum optics as constraining the energy dispersion relation in atom interferometers [9, 13], commutator measurements

on nanomechanical oscillator systems [12], observation of energy level shifts and modified tunnelling rates [10, 11], holographic noise measurements [14, 15] and the appearance of modified photon scattering rates [16].

Here we will focus on the approach developed in [9, 13], that proposes the test of quantum gravity induced energy dispersion modifications in the context of atom interferometry [17, 18]. This interferometry method, which relies on mapping acquired phase shifts to a well-controlled two-level quantum system, allows for the ultraprecise detection of spatial potentials and accelerations. Accordingly its applications are versatile, ranging from gravitational constant [18, 19] and recoil based fine structure measurements [20, 21] to the detection of magnetic field gradients and gravitational waves [22]. Replacing atoms by more massive particles is both interesting for testing the fundamental limits of quantum mechanics [9, 12] and in the analysis of decoherence effects [23, 24]. Of particular importance for the upcoming analysis, larger masses might be capable of enhancing Planck scale corrections. Color centers in diamond [25], such as nitrogen- or silicon-vacancy centers, form promising candidates for that task. As a specific example, we will focus on nanodiamonds comprising a nitrogen-vacancy center (NV<sup>-</sup>-center) (see figure 1), that does provide a well-controlled internal level-structure along with the possibility for optical initialization and readout of the spin qubit ground states [26]. Extraordinary long coherence times up to milliseconds [27] even at room temperature and combinations with dynamical decoupling methods [28] make them promising candidates as a solid state qubit. Furthermore, optical trapping [29, 30] and optical ground state manipulation [31, 32] have been demonstrated, which are important prerequisites for recoil based interferometry experiments. The interferometric application of nanodiamonds in a trapped gravimeter configuration has been proposed just recently [33].

This paper is organized as follows: We will start by introducing the modified energy dispersion relation along with the interferometric setup for its measurement in section I. Based on the interference signal and assuming various sources of noise and imprecisions, we then provide precision bounds in section II that may be anticipated in the determination of the quantum gravity modifications. Here we focus in particular on the mass scaling and a comparison between atomic and nanoparticle setups. Having identified the contribution for which the verification of their existence or non-existence seems feasible with nanodiamonds, we analyze the interference signal under the influence of gravitation and thermal motion in section III, showing that this contribution is in general unobservable as a result of suppression and decoherence mechanisms. As a viable solution we then provide in section IV a modified robust setup based on momentum inversion by gravitation, allowing to restore the perfect phase and visibility, that otherwise could just be achieved under challenging conditions. In section V we address the question whether massive particles and quantum optical schemes are suitable for tests of quantum gravitational corrections, thereby pointing out the still unsolved controversies that have emerged in the literature. Practical consideration as the combination with decoupling sequences, spatial decoherence, visibility reduction by imperfect pulses, time and pulse errors are discussed in section VI, focusing again on the particularities of nanoparticle setups. Following the main text, Appendix A provides the derivation of the interferometer phase based on a recently developed operator formalism [34], Appendix B gives an analysis of the developed robust stability setup and the required momentum conditions, and Appendix C discusses the difference of the modified energy dispersion approach to studies based on a modified commutator relation.

## I. MODIFIED ENERGY DISPERSION RELATION AND INTERFEROMETER PHASE

The approach developed in [9, 13] proposes the analysis of a modified energy dispersion, that in the non-relativistic limit takes the form

$$E(p) = \frac{p^2}{2m} + \xi_1 \frac{mcp}{2M_p} + \xi_2 \frac{p^2}{2M_p} \quad (1)$$

with  $p$  the particle momentum,  $m$  the mass and  $c$  the speed of light.  $\xi_1$  and  $\xi_2$  form free parameters, that have to be constrained by experiments. If the Planck scale plays a fundamental role both should be of order one. Indications for such linear and quadratic corrections in the particle momentum can be found in loop quantum gravity [35] and doubly special relativity approaches [7], respectively. In a broader context, the general ansatz (1), and in particular the  $\xi_2$  contribution, also serves as a test for Lorentz symmetry breaking [9, 36]. As pointed

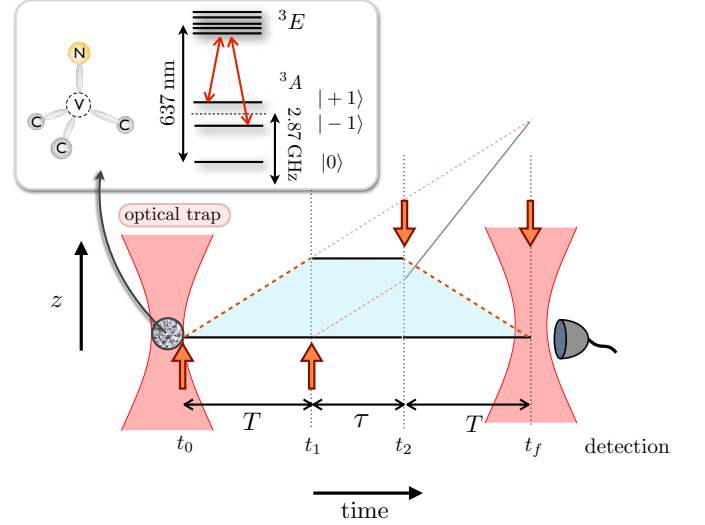


FIG. 1. **Ramsey-Bordé interferometer setup and NV-center energy levels.** An initially trapped nanoparticle undergoes the illustrated interferometer sequence where black lines correspond to the NV being in the ground state  $|g\rangle$  (e.g.  $|-1\rangle$  or  $|0\rangle$ ) and red dashed lines to the excited state  $|e\rangle$  (e.g.  $|+1\rangle$ ). Red arrows indicate  $\pi/2$ -laser Raman transitions, beam splitter operations with recoil transfer  $\hbar k$  in the corresponding laser directions. Those transitions can be realized using a  $\Lambda$ -scheme between the  $|+1\rangle$ ,  $|-1\rangle$  [37] or  $|0\rangle$ ,  $|+1\rangle$  [31]  $^3A$  ground states and an appropriate excited state of the manifold  $^3E$  with a photon recoil momentum  $\hbar k \simeq 2\hbar \cdot 2\pi/(637 \text{ nm})$ . The inset depicts the nitrogen vacancy center energy level structure.

out in [9, 13], which is exclusively based on an analysis of energy-momentum conservation, the phase of a Ramsey-Bordé interferometer as illustrated in figure 1, corresponds to the difference in the kinetic energy between the two paths. We will show in Appendix A, that for a closed path in momentum space and a potential at most linear in position (leading to an inertial force),  $H(\vec{p}, \hat{x}) = E(\vec{p}) + V(\hat{x})$  with  $V'(\hat{x}) = \text{const.}$ , the interferometer phase for an initial definite momentum state  $|\vec{p}\rangle$  is given by

$$\phi_{\text{int}} = \frac{1}{\hbar} \left[ \int_{t_0}^{t_1} \Delta E(\vec{p} - \nabla V(x) t', \hbar \vec{k}) dt' + \int_{t_2}^{t_f} \Delta E(\vec{p} - \nabla V(x) t', -\hbar \vec{k}) dt' \right] + \Delta\varphi \quad (2)$$

with the times defined as in figure 1,  $\Delta E(\vec{p}, \delta \vec{p}) = E(|\vec{p} + \delta \vec{p}\rangle) - E(|\vec{p}\rangle)$  and  $\Delta\varphi$  the laser and detuning phase with  $\Delta\varphi = [\varphi(t_f) - \varphi(t_2) + \varphi(t_1) - \varphi(t_0)] + \int_{t_0}^{t_1} \delta(t') dt' + \int_{t_2}^{t_f} \delta(t') dt'$ . Herein  $\delta$  denotes the laser detuning and  $\varphi(t)$  the absolute laser phase at time  $t$ . In the absence of an accelerating force, for equal time intervals  $T$  and a constant laser phase and detuning  $\delta$ , this reduces to  $\phi_{\text{int}} = 1/\hbar (\Delta E(\vec{p}, \hbar \vec{k}) + \Delta E(\vec{p}, -\hbar \vec{k})) T + \delta T$ . Upon completing the interferometer sequence, this phase is measur-

able as population oscillations with the phase dependent probability for finding the system in its initial ground state given by  $p_g = 1/8(1 + \cos(\phi_{\text{int}}))$ .

## II. PRECISION BOUNDS ON QUANTUM GRAVITY PARAMETERS

A variety of error sources and uncertainties, both of a practical and fundamental nature, limit the achievable precision in the interferometric determination of the quantum gravity parameters  $\xi_1$  and  $\xi_2$ . It will turn out that for  $\xi_2$  no gain can be expected in going for more massive particles such as nanodiamonds; from a practical perspective even the contrary holds true. On the other hand,  $\xi_1$  bounds benefit considerably from increasing masses and already a rather small nanodiamond size allows to verify its existence provided  $\xi_1 \sim 1$ . However, both for atoms and nanoparticles, such a  $\xi_1$  term will in general be suppressed by gravitational and thermal motion, the latter effect even scaling disadvantageously with increasing particle mass. Thus it is in general impossible to extract this data from existing interference experiments as has been proposed and performed in [9, 13], therefore, creating the need for a new setup and analysis as will be discussed in the upcoming sections.

The (perfect) external interferometric phase then takes the form

$$\phi = \frac{\hbar k^2}{m} T + \xi_1 \frac{m}{M_p} c k T + \xi_2 \frac{\hbar k^2}{M_p} T \quad (3)$$

and we will refer to the first term, the phase of an unmodified energy dispersion, as the ‘zero order’ contribution in what follows.

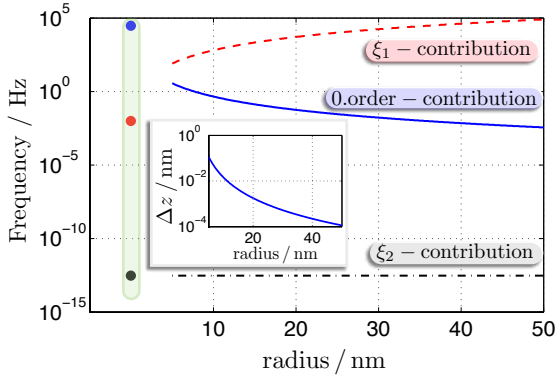


FIG. 2. **Frequency contribution and momentum splitting.** Interferometry phase frequency for different nanodiamond radii: The unperturbed recoil phase (zero order contribution, *blue solid*), the  $\xi_1$  quantum gravity correction (*red dashed*) and the  $\xi_2$  correction (*black dashed dotted*). The circles in the green area indicate the corresponding values for a Cs atom interferometer in the same colours. *Inset:* Maximal spatial separation of the interferometer paths for an interferometer time  $T = 100 \mu\text{s}$  and nanodiamonds.

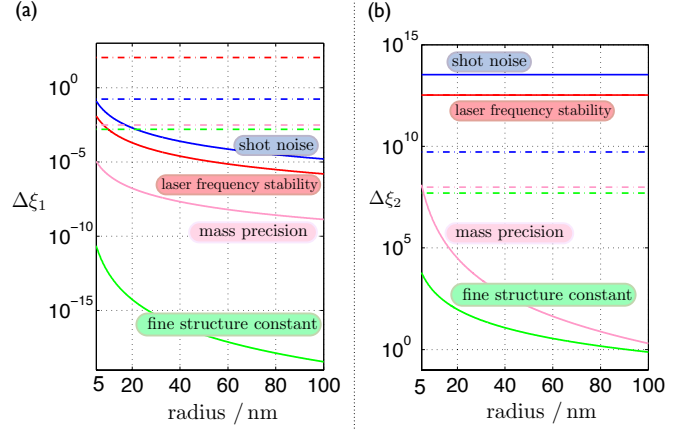


FIG. 3. **Precision bounds** on (a)  $\xi_1$  and (b)  $\xi_2$  arising from various error sources. Dashed dotted lines indicate the bounds for an atomic interferometry setup (Cs atoms). For the shot noise limitation we assume a number of  $N = 1000$  repetitions per data point and an interferometer time of  $T = 500 \mu\text{s}$  for nanodiamonds, whereas for Cs atoms  $N = 10^8$  and  $T = 10 \text{ ms}$  in accordance with recent atomic interference experiments [21] is assumed. The wavevector corresponds to a Raman transition recoil contribution with  $k \sim 2 \cdot 10^7 \text{ m}^{-1}$ . The mass precision for Cs atoms is given by [38]  $\Delta m_{\text{Cs}}/m_{\text{Cs}} = 10^{-9}$ , whereas for nanodiamonds a variance of  $\Delta m_{\text{NV}} = \pm m_{\text{C12}}$  corresponding to one carbon atom is assumed. The  $\Delta(\hbar/m_e)$  (fine structure) uncertainty has been extracted from electron magnetic moment anomaly measurements [39, 40] leading to  $\Delta(\hbar/m_e) = 5.9 \cdot 10^{-14} \text{ Js/kg}$ .

The magnitudes of the different phase contributions are depicted in figure 2 for different particle masses. Note in particular that for nanodiamonds the  $\xi_1$ -term, provided that it exists, forms the dominant phase contribution, whereas this role is ascribed to the zeroth order term for an atomic system. This turns out to be crucial for the error scaling in that uncertainties in the zero order phase term, denoted as ‘relative errors’, play a significant role for atomic systems whereas they are much less prominent for nanodiamonds. In particular for constraining  $\xi_1$  with nanoparticles, ‘relative errors’ play a minor role compared to ‘absolute errors’, the latter referring to mass and wavevector independent uncertainties as shot noise or frequency imprecisions. The mass and wavevector scaling for these two different types is given in table I along with the scaling of different error sources, the latter ones plotted for realistic experimental parameters in figure 3. As a consequence of the different error scaling, the absolute error scaling  $\Delta\xi_1 \propto 1/(mk)$  and  $\Delta\xi_2 \propto 1/k^2$  favours larger recoil contributions (wavevectors) for nanodiamonds, whereas the opposite conclusion can be drawn for atomic systems [13] based on the relative error scaling  $\Delta\xi_1 \propto k/m^2$ .

The  $\xi_1$ -bound benefits in both types of errors from an increasing mass. Strikingly, due to  $\xi_1$  being the dominant phase contribution for nanodiamonds, already a rather small radius of 5 nm might allow for the existence

Shot noise limit		$\Delta\xi_1^{\text{sn}} = \frac{1}{\sqrt{N}} \frac{M_p}{cT} \frac{1}{\mathbf{m} \mathbf{k}}$	$\Delta\xi_2^{\text{sn}} = \frac{1}{\sqrt{N}} \frac{M_p}{T \hbar \mathbf{k}^2}$
Laser frequency stability ( $\Delta\delta$ )		$\Delta\xi_1^{\text{lf}} = \frac{M_p}{c} \frac{1}{\mathbf{m} \mathbf{k}} \Delta\delta$	$\Delta\xi_2^{\text{lf}} = \frac{M_p}{\hbar} \frac{1}{\mathbf{k}^2} \Delta\delta$
Mass precision		$\Delta\xi_1^{\text{mass}} = \xi_1 \frac{\Delta m}{\mathbf{m}} + \frac{M_p}{\mathbf{m}^2} \frac{\hbar \mathbf{k}}{c} \frac{\Delta m}{\mathbf{m}}$	$\Delta\xi_2^{\text{mass}} = \frac{M_p}{\mathbf{m}} \frac{\Delta m}{\mathbf{m}}$
Precision of the fine structure constant / of ( $\hbar/m_e$ )		$\Delta\xi_1^\alpha = \frac{M_p m_e}{c} \frac{\mathbf{k}}{\mathbf{m}^2} \Delta\left(\frac{\hbar}{m_e}\right)$	$\Delta\xi_2^\alpha = \frac{M_p}{\mathbf{m}} \frac{1}{\hbar/m_e} \Delta\left(\frac{\hbar}{m_e}\right)$
General scaling	absolute value	$\Delta\xi_1 \propto 1/(m k)$	$\Delta\xi_2 \propto 1/k^2$
	relative value (zero order term)	$\Delta\xi_1 \propto k/m^2$	$\Delta\xi_2 \propto 1/m$

TABLE I. Imprecision bound formulas for the estimation of the parameters  $\xi_1$  and  $\xi_2$  due to different sources of imperfection. The last row indicates the general scaling with the particle mass  $m$  and the wavevector  $k$  for errors that are due to fluctuations of the zero-order phase (relative value) and mass and wavevector independent errors (absolute value), respectively. For typical nanodiamond sizes the zero-order contribution is very small rendering the absolute scaling the dominating one, whereas the inverse situation can hold true for atomic experiments.

or non-existence verification of such a  $\xi_1$ -term. The shot noise is, along with imprecisions in the laser detunings, the main and limiting error source, whereas fundamental knowledge of the fine structure constant will be very unlikely to limit the precision under realistic experimental conditions.

In contrast, the  $\xi_2$ -contribution exhibits a mass independent scaling for ‘absolute’ errors. From a practical point of view this favours atoms over nanoparticles, the former benefiting from the ability to realise parallel interferometric setups of up to  $\sim 10^8$  atoms [21], long coherence times  $T \sim 10$  ms, higher mass precisions originating in their elementary particle nature and elaborated techniques for large momentum transfers [21, 41, 42]. In particular the lack of parallelism for nanoparticle setups forms a challenging obstacle in overcoming a predominant shot noise error. Only for the much smaller relative errors can a mass favorable scaling be expected. In any case, a tight  $\xi_2$ -estimation remains a challenging task as any frequency imprecisions, e.g. the laser detuning stability, have to be compared to the very small  $\propto 10^{-13}$  Hz  $\xi_2$  contribution frequency (see figure 2). In previous work based on the experimental data of a Cs atom interferometer [20], the  $\xi_2$  parameter has been constrained to [13]  $\Delta\xi_2 \simeq 2.6 \cdot 10^9$ , and an improvement of one order of magnitude  $\Delta\xi_2 \simeq 3 \cdot 10^8$  can be obtained from more recent experimental data based on Rb-atoms [21], still far from verifying or falsifying the existence of such a quantum gravity correction.

### III. CAN A $\xi_1$ -TERM BE OBSERVED IN EXPERIMENTS?

As outlined in the previous section, it is merely the  $\xi_1$  contribution that may gain advantage from an increased mass, in addition, it is the quantity for which the verification of its existence or non-existence seems feasible. However this term exhibits two crucial drawbacks: First, there remains in general a dependence on the absolute particle momentum  $\vec{p}$  even for a perfect interferometer sequence. This resembles the situation of open inter-

ferometers, in which by averaging over an initial thermal distribution of particle momenta, decoherence, and therefore a reduction of the interferometer visibility, may be anticipated. Second, contrary to the phase contributions quadratic in momentum, the impact of gravitation on the linear  $\xi_1$  term does not appear as a separate phase factor nor can it be eliminated by choosing the recoil momentum orthogonal to the gravitation direction. In contrast, pure gravitation will suppress the  $\xi_1$  phase term contribution. Therefore, in the absence of a specific preparation of the interferometer sequence, the coherent  $\xi_1$  contribution appearing in (3) will in general be unobservable. Whereas the thermal phase suppression scales  $\propto \sqrt{m}$ , thus leading to more restrictive prerequisites for increasing mass, the equally challenging gravitational counterpart turns out to be mass independent. In the following we will begin by analyzing the phase term for a constant non-zero initial momentum, which will lead to a description of the phase-term behaviour for a thermal particle along with conditions for its observation. Next, the influence of gravitation will be considered in more detail with a subsequent discussion of the influence of both gravitation and thermal motion.

#### 1. $\xi_1$ -phase and suppression for a constant momentum

The external phase contribution of the  $\xi_1$ -term according to (1) & (2), takes the following form

$$\phi_{\xi_1} = \mu \left( \int_{t_0}^{t_1} |\vec{p}_1(t') + \hbar \vec{k}| - |\vec{p}_1(t')| dt' + \int_{t_2}^{t_f} |\vec{p}_2(t') - \hbar \vec{k}| - |\vec{p}_2(t')| dt' \right) \quad (4)$$

with  $\mu = \xi_1 m c / (2\hbar M_p)$ , the times as defined in figure 1 and we will assume that  $t_1 - t_0 = t_f - t_2 = T$ . As a special, and particularly relevant case, we will consider the situation of a constant momentum in time, but allow for different momenta  $\vec{p}_1$  and  $\vec{p}_2$  in the first ( $[t_0, t_1]$ ) and second ( $[t_2, t_f]$ ) interferometer cycle, respectively. With



$$|p_1|, |p_2| \gg \hbar k$$

$$\phi_{\xi_1} \simeq \mu T \left\{ |\hbar k| (\cos \theta_1 - \cos \theta_2) + \frac{|\hbar k|^2}{2} \left[ (1 - \cos^2 \theta_1) \frac{1}{|p_1|} + (1 - \cos^2 \theta_2) \frac{1}{|p_2|} \right] \right\} \quad (5)$$

where  $\cos \theta_i = p_i^z / |p_i| \text{sgn}(\hbar k)$  with  $\theta_i$  the angle between the momentum and recoil. The second contribution in (5) is purely decaying to zero in this limit. Therefore a significant phase, characterized by a non-zero value of the first contribution, can only be observed if  $\theta_1 \neq \theta_2$ , that is if there exists a change in the momentum direction  $\vec{p}$  from the first to the second cycle. This latter fact will be used to create an experimental setup in a stability configuration in section IV.

Let us first consider the case of equal momenta  $\vec{p}_1 = \vec{p}_2 = \vec{p}$ , that e.g. corresponds to a particular momentum state out of a thermal distribution. The phase contribution (4) for different momentum magnitudes and orientational configurations, is shown in figure 4(a) and reveals a purely decaying behaviour, such that a significant phase contribution in that regime can be expected only in the limit  $|p| \ll |\hbar k|$ .

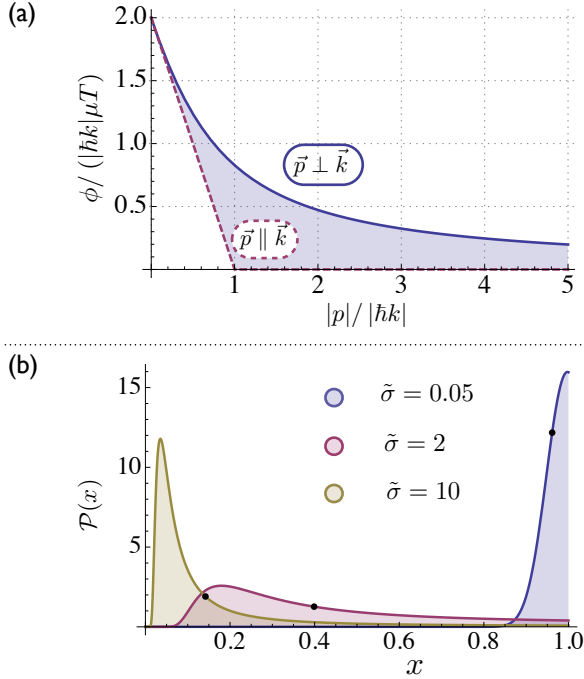


FIG. 4. **Momentum phase suppression and frequency distribution** (a) Suppression of the  $\xi_1$ -phase contribution for an initial non-zero momentum  $\vec{p}$  (constant during the interferometric cycle) and different orientations to the recoil contribution  $\hbar \vec{k}$ . Intermediate orientations do fall into the blue shaded region. (b)  $\xi_1$ -term frequency distribution for the dimensionless frequency  $x = \omega / (2\mu\hbar k)$  and a Gaussian momentum distribution with different variances  $\tilde{\sigma} = \sigma / (\hbar k)$  and assuming  $\vec{p} \perp \hbar \vec{k}$ .

## 2. Thermal momentum distribution

Following the previous discussion, the  $\xi_1$ -phase term dependence on the initial particle momentum is responsible for both a suppression of the phase contribution (figure 4(a)) and decoherence in case of an initial momentum distribution.

Now assuming a motional thermal state of the interferometric particle, its momentum will be distributed according to a Gaussian distribution

$$\mathcal{P}(p_\alpha) = \langle p_\alpha | \rho_{th} | p_\alpha \rangle = \frac{1}{\sqrt{2\pi\sigma^2}} e^{-\frac{p_\alpha^2}{2\sigma^2}} \quad (6)$$

with  $\alpha \in x, y, z$  referring to the spatial direction and  $\sigma^2 = \langle \hat{p}^2 \rangle - \langle \hat{p} \rangle^2$  the momentum variance given by  $\sigma^2 = \hbar/2m\omega_\alpha(1+2n_{th})$  for a thermal harmonic oscillator state with frequency  $\omega_\alpha$  and a thermal population of  $n_{th} = (\exp(\hbar\omega_\alpha/(k_B T)) - 1)^{-1}$ . This reduces to the Boltzmann distribution  $\sigma^2 \simeq m k_B T$  for  $k_B T \gg \hbar\omega_\alpha$  or equivalently for a free particle. In any limit the momentum variance, responsible both for phase suppression and fluctuations, grows with increasing mass  $\sigma \propto \sqrt{m}$ , and consequently makes a phase observation more challenging for massive particles.

Three different regimes can be identified, assuming that an individual momentum state  $i$  out of the distribution leads to a  $\xi_1$ -phase contribution  $\phi_{\xi_1}^i = \omega_i T$ :

For  $|\sigma| \ll |\hbar k|$  the frequency contribution of any of the thermal momentum states is approximately given by  $\omega_i \simeq 2\mu\hbar k$ , thus approaching the perfect phase given in (3). As thermal fluctuations around this optimal frequency are small, decoherence only has a negligible influence.

In contrast, for  $|\sigma| \simeq |\hbar k|$  all possible frequencies  $\omega_i \in [0, 2\mu\hbar k]$  appear with almost equal probability, therefore leading to the largest frequency variance and a decay of interference fringes. Consequently, coherent phase contributions cannot be observed in that regime.

Last, in the limit  $|\sigma| \gg |\hbar k|$  the phase suppression with increasing momentum is responsible for a dominant frequency contribution  $\omega_i \simeq 0$ . As only very few momentum states have significant non-zero frequencies, the frequency variance decreases again. Thus no coherent  $\xi_1$ -oscillations can be observed in that regime, but at the same time decoherence decreases with increasing  $\sigma$ , therefore not disturbing the observation of other phase contributions on that timescale (e.g. the zero-order contribution).

Figure 4(b) illustrates the frequency distribution for different variances  $\tilde{\sigma} = \sigma / (\hbar k)$  and the dimensionless frequency  $x = \omega / (2\mu\hbar k)$ ,

$$\mathcal{P}(x) = \frac{1}{\sqrt{2\pi\tilde{\sigma}^2}} \left( 1 + \frac{1}{x^2} \right) \exp \left( -\frac{1}{2\tilde{\sigma}^2} \frac{1}{4} \left( \frac{1}{x} - x \right)^2 \right) \quad (7)$$

based on the thermal momentum distribution (6), which reveals exactly the behaviour previously discussed. Figure 5(a) presents an analysis of the  $\xi_1$  interference fringes

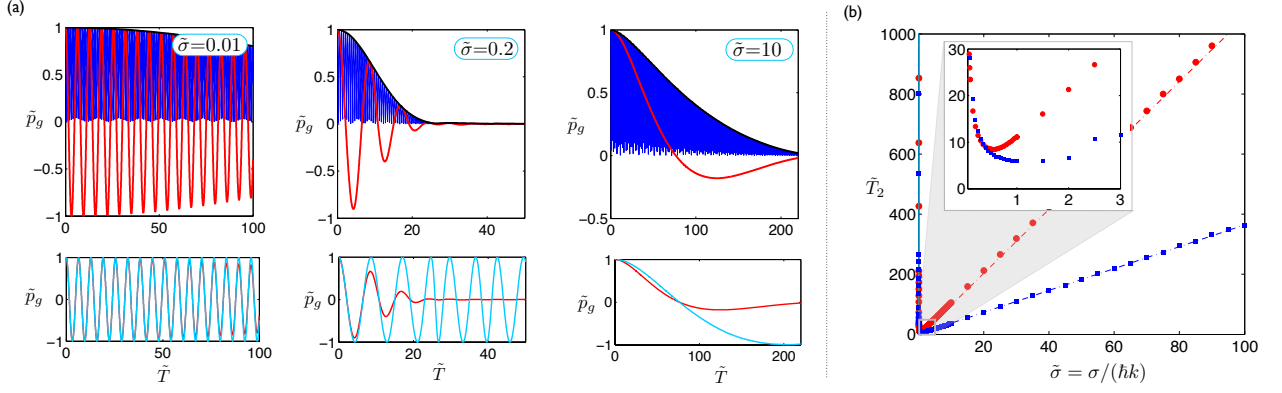


FIG. 5. **Thermal influence on the  $\xi_1$ -contribution.** (a)  $\xi_1$ -interference contribution (red)  $p_g = \frac{1}{8} (1 + \tilde{p}_g)$  for different values of the thermal momentum variance  $\tilde{\sigma} = \sigma/(\hbar k)$  plotted versus the dimensionless time  $\tilde{T} = 2\mu(\hbar k)T$ . A fast oscillation frequency, whose absolute value contribution is plotted here, has been added artificially to the phase (dark blue) to extract the decoherence decay envelope (black). The lower panel shows the coherent phase contribution (light blue) with subtracted decay envelope and the actual observed  $\xi_1$ -interference contribution (red). (b) Dimensionless coherence time  $\tilde{T}_2 = 2\mu\hbar k T_2$  vs the variance for a three (red) and one-dimensional (blue, in an orthogonal direction to  $\hbar k$ ) thermal distribution out of a thermal Monte Carlo simulation. The minimal value is obtained for  $\tilde{\sigma} \simeq 1$  and a linear behaviour in  $\tilde{\sigma}$  and  $1/\tilde{\sigma}$  is observed in the limit  $\tilde{\sigma} \gg 1$  and  $\tilde{\sigma} \ll 1$ , respectively, that has been fitted to  $\tilde{T}_{2,\tilde{\sigma} \gg 1}^{3d} \simeq 10.63 \tilde{\sigma} - 9.2$ ,  $\tilde{T}_{2,\tilde{\sigma} \ll 1}^{3d} \simeq 2.13 \cdot 1/\tilde{\sigma} + 1.8$ ,  $\tilde{T}_{2,\tilde{\sigma} \gg 1}^{1d} \simeq 3.64 \tilde{\sigma} + 0.7$  and  $\tilde{T}_{2,\tilde{\sigma} \ll 1}^{1d} \simeq 2.67 \cdot 1/\tilde{\sigma} + 1.2$ .

$p_g = \frac{1}{8} (1 + \tilde{p}_g)$  for different  $\tilde{\sigma} = \sigma/(\hbar k)$ -regimes and a three-dimensional thermal distribution, extracting the coherent contribution and the decay envelope. Only the regime  $\tilde{\sigma} \ll 1$  is appropriate to analyze the  $\xi_1$ -phase as expected and there is a clear significance of the previously described regimes. We note that in the overdamped regime a coherent oscillation on the  $T_2$ -timescale emerges, representing the very small non-zero average frequency in that regime. The extracted coherence times  $T_2$  are shown in figure 5 (b), being smallest in the  $\tilde{\sigma} \sim 1$  regime and increasing linearly with  $\tilde{\sigma}$  and  $1/\tilde{\sigma}$  in the  $\tilde{\sigma} \gg 1$  and  $\tilde{\sigma} \ll 1$  limit, respectively. Importantly whereas the relevant regime depends only on the value of  $\tilde{\sigma} \propto \sqrt{m}$ , the absolute timescales are proportional to  $m^{-1}$  as expected by the mass dependent prefactor  $\mu$  in (4). Additional non-zero average particle momenta  $\langle p_i \rangle = p_0 \neq 0$  will push the interferometer further into the  $\tilde{\sigma} \gg 1$  regime as is readily seen from figure 4 (a), and therefore into a regime where neither a coherent nor a decoherent signature of the  $\xi_1$ -term will be observed, which might lead to the premature conclusion that such a term does not exist.

Typical values for the momentum variance  $\tilde{\sigma}$  and the coherence time  $T_2$  are shown in table II. Originating from the small recoil momentum transfer those values are in general located far in the overdamped  $\tilde{\sigma} \gg 1$  regime, except for challenging low temperatures. As a consequence of the variance scaling with the particle mass, reaching the regime of coherent oscillations ( $\tilde{\sigma} \ll 1$ ) seems very hard for more massive particles and might at most be possible for small nanodiamond radii ( $\sim 5$  nm), following a harmonic ground state cooling with subsequent adiabatic relaxation of the trap frequency. Note that increasing the beam-splitter momentum  $\hbar k$  [21, 41, 42], recalling

		r=5 nm	r=50 nm	Cs atom
HO ground state	$\tilde{\sigma}$	0.37	12	$4 \cdot 10^{-3}$
( $\omega = 2\pi \cdot 1$ Hz)	$T_2/s$	0.03	$2.5 \cdot 10^{-4}$	$9 \cdot 10^3$
T=4 $\mu$ K	$\tilde{\sigma}$	153	$5 \cdot 10^3$	1.7
	$T_2/s$	3.2	0.1	$3.6 \cdot 10^2$
T=1 mK	$\tilde{\sigma}$	$2 \cdot 10^3$	$8 \cdot 10^4$	27
	$T_2/s$	52	1.6	$4.5 \cdot 10^3$
T=10 K	$\tilde{\sigma}$	$2 \cdot 10^5$	$8 \cdot 10^6$	$2.6 \cdot 10^3$
	$T_2/s$	$5 \cdot 10^3$	$1.6 \cdot 10^2$	$4.7 \cdot 10^5$

TABLE II. **Thermal momentum variance and  $T_2$ -time** Thermal momentum variance  $\tilde{\sigma} = \sigma/(\hbar k)$  for  $k = 1.9 \cdot 10^7 m^{-1}$  corresponding to a 637 nm Raman transition and the corresponding  $T_2$ -time for different nanodiamond radii / a Cs atom and different temperatures. The first row corresponds to the quantum fluctuations of an harmonic oscillator (HO) ground state with frequency  $\omega$ . Note that the variance, which determines the regime as outlined in the main text, scales  $\propto \sqrt{m}$ , whereas the absolute timescale is proportional to  $1/m$  reflecting the mass dependence of the  $\xi_1$ -contribution term.

that  $\tilde{\sigma} = \sigma/(\hbar k)$ , can help in the achievement of a coherent regime.

### 3. Influence of gravitation

For phase contributions quadratic in the momentum, gravitation leads at most to an additional phase factor (see also Appendix A). In the case of the  $\xi_1$ -contribution

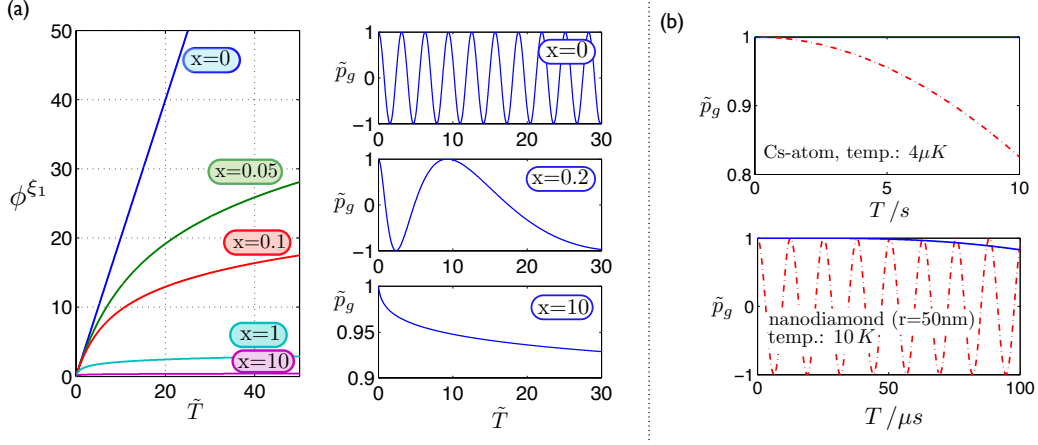


FIG. 6. **Gravitational suppression and combined simulations.** (a) Influence of gravitation on the  $\xi_1$ -phase (left) and oscillation fringe suppression  $p_g = 1/8(1 + \tilde{p}_g)$  for different values of  $x = M_p g/(\hbar k^2 c)$ . A zero initial momentum is assumed and the gravitational direction has been chosen orthogonal to the recoil momentum. (b) Real value  $\xi_1$ -simulations combining gravitation ( $\vec{g} \perp \vec{k}$ ) and thermal effects for Cs and a nanodiamond with radius 50 nm (blue lines) and the perfect unperturbed situation for comparison (red lines). For Cs gravitation dominates whereas in the nanodiamond case both thermal and gravitational effects are of the same magnitude. This latter situation leads to an enhanced decoherence compared to the value given in table II as is explained in the main text.

however, it can have a destructive effect on the observation of the phase itself, as seen in figure 4(a). With no additional pulse sequences involved, the gravitational effect can be described by choosing  $\vec{p}_1(t') = \vec{p}_2(t') = \vec{p}^0 - m\vec{g}t'$  in (4), with a potential non-zero initial momentum  $\vec{p}^0$ , that we will set to zero for now. Such a situation is characterized by the dimensionless quantity  $x = [mg/(\hbar k)] / [2\mu\hbar k] = M_p g/(\hbar k^2 c)$ , that corresponds to the ratio between suppression and coherent (optimal) phase evolution frequency. As both quantities scale proportional to the mass, this regime characterizing factor is mass independent, i.e. there exists no advantage concerning the fringe observation by changing the mass. For  $x > 1$  the overdamped regime is reached, in which coherent oscillations are essentially suppressed, and the phase can be approximated by (in the limit  $x\tilde{T} \gg 1 \Leftrightarrow mgT \gg \hbar k$ )

$$\phi_{\xi_1} \simeq \frac{1}{2x} \left[ \frac{1}{2} + \log(4x\tilde{T}) \right] \quad (8)$$

with  $\tilde{T} = 2\mu\hbar k T$ . In contrast  $x \ll 1$  forms the desired regime in which gravitation is merely a perturbative factor to the  $\xi_1$ -phase evolution. However for a Raman recoil contribution with wavelength  $\lambda = 637 \text{ nm}$ ,  $x = 1.7 \cdot 10^4$ , a value located deep in the suppression regime independent of the particle's size. A challenging recoil of  $\sim 10^2 \hbar k$  would be required to turn this into a coherent oscillatory  $x \ll 1$  regime, potentially feasible with atomic systems [21, 41, 42]. Figure 6 illustrates this phase behaviour for different  $x$ -values showing a slowdown of the accumulated phase and consequently a fringe suppression for increasing magnitudes. For realistic  $x$ -values, no oscillations would be observable at all.

#### 4. Combining both effects

Up to now, the thermal and gravitational influences have been analyzed separately. The combination of both is illustrated in figure 6(b), for the case of a Cs atom and a nanodiamond under realistic experimental temperatures. As expected,  $\xi_1$ -oscillations are highly suppressed. In cases where  $\chi_{\text{grav}} \equiv 2mgT \gg \sigma$ , i.e. when the gravitational momentum gain is large compared to the typical thermal momentum magnitudes, the situation is well described by the pure gravitational case as is the case for the Cs atom simulation ( $\tilde{\chi}_{\text{grav}} = \chi_{\text{grav}}/(\hbar k) \sim 2 \cdot 10^4$ ,  $\tilde{\sigma} = 1.7$ ). In the opposite regime  $\chi_{\text{grav}} \ll \sigma$  the thermal description holds. However, in an intermediate regime of comparable magnitudes the behaviour can deviate from the individual ones. This is best understood in the (relevant)  $|p| \gg |\hbar k|$  regime approximated in (5). For a significant phase the first non-decaying term, reflecting the parallel component, has to be non-zero. This is only the case if there occurs a momentum angle change with respect to the recoil momentum axis in between the first and second interferometric cycle. For a purely thermal or gravitational situation this angle remains fixed. However combining both, gravitation will induce a change in the relative  $p_z$  component, leading to  $\theta_1 \neq \theta_2$  for any thermal  $\vec{p}$  non-parallel to the gravitational direction. This leads to a significant first term phase contribution in the limit when both the thermal momentum and the gravitational momentum gain are of the same magnitude. In the absence of any initial effective momentum this does lead to a fluctuating contribution ( $\langle \cos \theta_1 - \cos \theta_2 \rangle = 0$ ), resulting in an increased decoherence instead of a coherent contribution, an effect that can be seen in the nanodiamond simulation of figure 6(b). In that case  $\tilde{\chi}_{\text{grav}} \simeq 2 \cdot 10^6$

$\sim \tilde{\sigma} = 8 \cdot 10^6$ ; for a purely thermal coherence a much smaller decay rate would have to be expected from table II. Note however, that a non-zero initial momentum combined with gravitation can lead to a significant real coherent evolution based on the same enhancement mechanism, a discussion that will be the subject of the next section.

In summary, only two situation will lead to the observation of a significant coherent  $\xi_1$ -phase contribution: The first is cooling of the particle to a regime  $\tilde{\sigma} \ll 1$ , requiring ground state cooling for trap frequencies  $< 1\text{Hz}$  in the typical nanodiamond regime, along with performing the setup in a gravitation free space. Both of those conditions could be significantly relaxed by increasing the recoil transfer of the beam splitter operation by at least a factor of  $10^2$ . Second, preparing the system in a non-zero initial momentum state non-parallel to the gravitation direction, with both the gravitational momentum transfer and the initial momentum being of the same magnitude and exceeding the momentum variance for a sufficiently long coherence time.

#### IV. STABILITY CONFIGURATION FOR THE $\xi_1$ -MEASUREMENT

As outlined in the previous section, a change in the momentum direction relative to the recoil orientation  $\vec{k}$  within the interferometric sequence, can lead to the appearance of a significant non-zero phase term even in the presence of a large absolute momentum value. In the following the terms ‘parallel’ and ‘orthogonal’ will always refer to the momentum relative to the recoil direction  $\vec{k}$  of the first interferometric cycle  $[t_0, t_1]$ , unless stated otherwise. Whereas for the orthogonal component each individual cycle phase contribution decays to zero with increasing  $|p|$ , for the parallel component the combination of both cycles is crucial. Changing the direction of the initial momenta, such that  $\vec{p}_1^0 \neq \vec{p}_2^0$  (see figure 7), or more precise changing the angle to the recoil term, will lead to a momentum independent contribution (see (5)). This fact can be used to construct a regime, in which the  $\xi_1$ -phase can be observed despite thermal and gravitational influences. For static momenta, the optimal condition can be identified from (5), following as

$$\vec{p}_1^0 \uparrow \uparrow \vec{k} \quad \&\& \quad \vec{p}_2^0 \uparrow \downarrow \vec{k} \quad (\Leftrightarrow \vec{p}_1^0 \uparrow \downarrow \vec{p}_2^0) \quad (9)$$

i.e. the first initial momentum is parallel to the recoil whereas there occurs a change in the momentum direction in between the two interferometer cycles, such that the second initial momentum is antiparallel to the first one (and parallel to the second recoil direction). In that case  $\phi_{\xi_1} = \mu t 2 \hbar k$ , which corresponds to the optimal phase (3), the same as would appear in the absence of any momenta except the beam splitter operations. We will call this regime the ‘stability regime’ because, once the parallel and antiparallel condition is reached, the phase

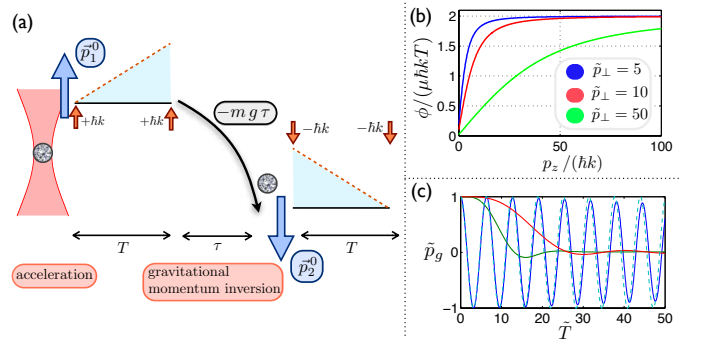


**FIG. 7. Stability regime setup and phase recovery.** (a) Interferometric setup in the stability  $\xi_1$ -regime using gravitation for the momentum inversion. Initially a large recoil parallel momentum is transferred that can be performed within the optical trap. The free evolution time  $\tau$  in between the first and second sequence is responsible for the momentum inversion to an antiparallel regime. (b)  $\xi_1$ -phase for different values of the recoil orthogonal momentum  $\tilde{p}_\perp = p_\perp / (\hbar k)$ , leading to a suppression of the phase term, vs. an increasing parallel component  $p_{1,z}^0 = -p_{2,z}^0 = p_z$ . For  $|p_z| \gg |p_\perp|$  the stability regime is reached leading to the maximal optimal phase  $\phi_{\xi_1} = 2\mu \hbar k T$ . (c) Recovery configuration for  $\tilde{\sigma} = \sigma / (\hbar k) = 100$  and  $x = M_p g / (\hbar k^2 c) = 5$  in a configuration as depicted in (a).  $\tilde{t}$  denotes the dimensionless time  $\tilde{t} = 2\mu \hbar k t$ . Herein  $\tilde{p}_z^0 = p_z^0 / (\hbar k) = x \tilde{T} + (1 + \zeta \sqrt{2}) \tilde{\sigma}$  with  $\zeta = 5$  guaranteeing that the parallel component exceeds the perpendicular one most likely by a factor of  $\zeta = 5$  even at its smallest value at time  $T$  (assuming equal momentum variances  $\tilde{\sigma}$  in all spatial directions). The time  $\tau$  is chosen to allow for the same ratio in the second cycle, such that  $p_{2,z}^0 \simeq -\zeta \sqrt{2} \sigma$ . Blue lines show the  $\xi_1$  population oscillations in the recovery regime, light blue dashed lines the optimal phase without any disturbance, whereas red and green lines correspond to a non-adjusted ‘normal’ configuration with  $\tau = 0$  and  $\vec{p}_1^0 = 0$  for  $\vec{g} \perp \vec{k}$  and  $\vec{g} \parallel \vec{k}$ , respectively.

is highly stable and independent of the absolute momentum value, thereby making it stable against decoherence. Moreover this holds for any momentum even outside the  $|p| \gg |\hbar k|$  regime as will be shown in Appendix B. As can be seen, one could anticipate from (5) that a configuration  $\vec{p}_1^0 \uparrow \downarrow \vec{k}$  and  $\vec{p}_1^0 \uparrow \downarrow \vec{p}_2^0$  will lead to the same phase magnitude despite a negative overall sign, however such a regime is only momentum independent in the limiting case of the validity of (5). A configuration based on changing the parallel momentum direction in between the first and second cycle, is demonstrated in figure 7(b). Once the parallel regime is approached, i.e. the parallel momentum dominates the orthogonal component, the latter being purely responsible for suppression, the phase is recovered up to its optimal unperturbed value.

Experimentally, one has merely to guarantee the parallel condition along with a momentum direction change in between the two cycles involved. The first one can be arranged by an initial parallel momentum sufficiently large such that it exceeds the momentum gain of gravitation



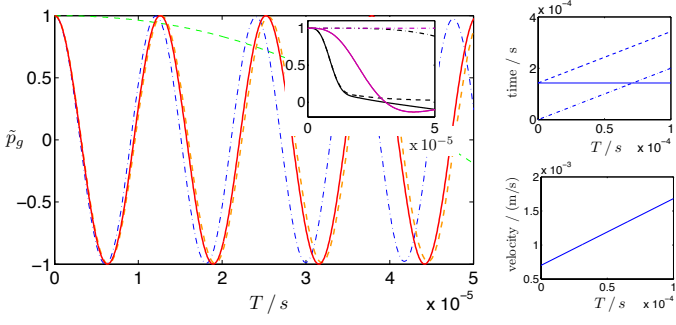


**FIG. 8. Phase recovery for a 50 nm nanodiamond.** Phase recovery scheme simulation for a setup as depicted in figure 7 (a), a nanodiamond of radius 50 nm, and a parallel component exceeding the orthogonal one upon design by a factor  $\zeta = 5$  as defined in the caption of figure 7. The temperature has been chosen as 1 mK in order to make the thermal momentum variance comparable to the gravitational momentum gain. *Left:* Population oscillations for the combination of zero order and  $\xi_1$ -term (blue dashed dotted), the  $\xi_1$ -term alone (red solid) and the zero order contribution alone (green dashed). Orange dashed lines indicate the perfect  $\xi_1$  situation in the absence of thermal noise and gravitation. *Inset:* Interference oscillations in the absence of a specifically designed recovery sequence for the same parameters, but  $\tau = 0$  and  $p_1^0 = 0$ . Black and pink lines correspond to  $\vec{g} \parallel \vec{k}$  and  $\vec{g} \perp \vec{k}$ , respectively, whereas solid, dashed and dashed dotted refers to the combination of the zero order and  $\xi_1$ -term, the  $\xi_1$  term alone and the zero order contribution alone, respectively. *Upper right:* The waiting time  $\tau$  (solid), the total interferometric time ( $2T + \tau$ ) in the recovery setup (dashed) and the interferometric time without a recovery cycle ( $2T$ ) (dashed dotted) for different interference times  $T$ . *Lower right:* Initially transferred velocity parallel to the recoil vs  $T$ .

and the thermal momentum variance  $\sigma$ . The second condition will require a directional momentum change during the intermediate time period  $\tau$ , that can be obtained by an external acceleration or making use of gravitation. We will focus on the latter, as a momentum transfer by e.g. laser pulses may be prone to destroy the spatial superposition state by e.g. incoherent photon scattering. This leads to a possible setup as depicted in figure 7 (a) in a configuration such that  $\vec{g}$  is antiparallel to the initial recoil direction. An initial momentum is transferred such that its magnitude exceeds the thermal variance and gravitation,  $|\vec{p}_1^0| > \sigma, 1/2 \chi_{\text{grav}}$ , ensuring the parallel regime, followed by a free evolution sequence  $\tau$  in which gravitation provides the change to an antiparallel configuration with  $|\vec{p}_2^0| > \sigma$ . For such a gravitational scheme to work, the thermal variance should be at most comparable (or smaller) in magnitude to the gravitational momentum gain  $\tilde{\sigma} \lesssim |\chi_{\text{grav}}|$  as otherwise the intermediate time period would have to be much longer than the interferometer time ( $\tau \gg T$ ), which is very impractical and might even be impossible within the internal  $T_2$  coherence time. This will in general imply an initial motional particle cooling [43] more restrictive for increasing particle mass. Figure 7 (c) demonstrates that mech-

anism in dimensionless units. For a parallel momentum component exceeding the orthogonal fluctuating thermal ones by at least a factor of five, an almost perfect recovery of coherent oscillation fringes is achieved. A realistic example is provided in figure 8 for a nanodiamond of radius 50 nm. Here an initial cooling to a temperature of 1 mK along with an initial velocity transfer of the order of 1 mm/s, allows for the observation of well-defined coherent interference fringes on a timescale of 200  $\mu\text{s}$ , within range of the NV-center coherence time. This would be a sufficient test for the existence of such a term.

Note that, by working in the parallel regime, in particular in a regime with the gravitation being parallel to the recoil direction, the zero order phase contribution will be altered as well, namely by an additional phase  $\Delta\phi_0 = (1/m)\vec{k} [\vec{p}_1^0 - \vec{p}_2^0] T$ . This term will have to be accounted for in a proper determination of  $\xi_1$ , requiring a precise knowledge of the initial momentum and the gravitation direction. To avoid that additional change one could also use alternative momentum schemes by choosing the gravitation orthogonal to  $\vec{k} \parallel \vec{p}_1^0$ , with the initial momentum subsequently changed by at most a  $\pi/2$  rotation for the second cycle under the influence of gravitation; however, with the drawback that such a regime is only approximately momentum-independent for  $|p| \gg |\hbar k|$  and according to (5) the maximal phase is one half of the one in the parallel gravitational approach.

## V. CAN QUANTUM GRAVITY EFFECTS BE EXPECTED IN INTERFEROMETRIC SETUPS OF MASSIVE PARTICLES?

The question whether quantum gravitational effects can be expected in such a quantum optical interferometric setup turns out to be very controversial. Whereas an energy dispersion modification has been proposed in many theories to date [6, 7, 35], its inclusion into the ‘test framework’ of standard quantum mechanics [13] remains debatable. In light of the incompleteness and controversies of existing quantum gravity theories, probing such a small detail in a large framework seems a promising starting point, that can both help to validate and promote a better understanding of Planck scale physics. However one should keep in mind, that a theory of quantum gravity is much more than merely a modified energy dispersion relation or a modified commutator. It should in addition specify the underlying metric, the behaviour under transformations that might go along with a deformed Poincaré symmetry, a kinematic description of the equations of motion, and an interpretation of the physically relevant coordinates and observables [2].

The question remains whether massive particles are appropriate for testing quantum gravity. As for macroscopic bodies the proposed energy dispersion corrections would be large, what is unobserved on a macroscopic scale, it is a natural assumption to introduce a restriction to particle sizes that do behave ‘quantum mechan-

ically' [13]. Note that the proposed energy dispersion corrections (1) constitute a perturbative expansion for small masses and would consequently not be valid in the macroscopic limit anyway. Even more delicate, a consistent framework would most probably require a modification of special relativity, and for a curved metric this will result in a non-linear momentum addition law. This can be motivated by the fact, that a minimal lengthscale maintains a fundamental role only if it is observer independent, contradictory to the standard framework of special relativity [6, 7]. As a modified velocity addition law has been the consequence of defining a fundamental velocity in special relativity (the speed of light), it is not surprising that introducing in addition a fundamental lengthscale can lead to a modified momentum addition. Such a non-linear addition will however lead to a scaling problem as an iteration of a correction quadratic in the momentum scales quadratically with the number of constituents and will eventually become significantly large in contradiction to the 'macroscopic world' observation. This is well-known in the literature as the 'soccer ball problem' [2, 44, 45], such that a restriction of the theory to 'fundamental particles' has been stated by many authors, even though this notion remains imprecise. A possible solution for composite particles of  $N$  constituents has been proposed by replacing the Planck mass  $M_p$  by  $N M_p$  [44, 45]; an approach that would not result in any advantages for nanoparticles over atoms in testing quantum gravity. Last, there have been some proposals, that the quantum gravity corrections depend on the mass density rather than the absolute particle mass [46]. Remarkably, apart from all those controversies, a test of the energy dispersion relation, will serve a test for the validity of special relativity even in a broader context [9, 36].

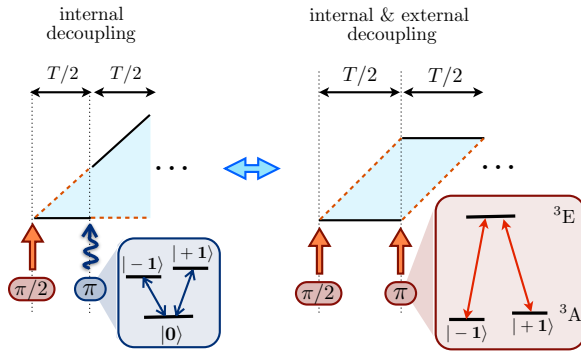


FIG. 9. **Pulsed decoupling scheme:** *Left:* Internal decoupling by a recoil free (microwave-)  $\pi$ -pulse. *Right:* Decoupling of the internal and external degrees of freedom by a Raman-(recoil)-laser pulse, leading to an accelerometer (Gravimeter) interferometry setup. Red arrows indicate Raman laser transitions whereas blue wavy arrows represent microwave transitions. Black and red dashed lines represent the initial ground and the excited state, respectively.

## VI. INTERFEROMETRY WITH MASSIVE PARTICLES AND DECOHERENCE

Here we briefly discuss practical issues of such an interferometric implementation based on nanoparticles: The decoupling from decoherence, collisional decoherence, imperfect pulses and time constraints and their impact on the interference fringe visibility. We will focus here on the robust stability regime; however as these effects are either general or mainly based on the zeroth order phase term, these results also hold true for other interferometric applications with nanoparticles and even the same scaling properties can be expected for different types of interferometers.

Decoherence decoupling schemes [28] for the internal degrees of freedom, crucial to reach significant  $T_2$ -coherence times and in addition removing quasi-static energy shifts, can be implemented by (almost) recoil free microwave  $\pi$ -pulses within the ground state triplet, as shown in figure 9. Note that recoil based  $\pi$ -pulses, obtained in analogy to the beam splitter interactions, would lead to the well-known gravimeter configuration [18, 19, 34]. This latter setup, unsuitable for the anticipated task, reveals a decoupling in both the external and internal degrees of freedom, which makes it only sensitive to accelerations ( $V'(x) \neq 0$ ).

Figure 10 analyzes several sources of decoherence and visibility loss. Following the fact that for recoil based beam splitters the space-time area scales inversely with the particle mass  $\propto 1/m$  and that the thermal velocity variance  $\sigma_v \propto 1/\sqrt{m}$ , these decoherence effects show a favorable scaling with increasing mass. Background gas collision induced decoherence, the prominent spatial decoherence source [23] for nanoparticles, is illustrated in figure 10 (a) for different pressures and particle sizes. Here a gas particle momentum change  $\Delta \vec{p}$  during the scattering process will lead to a (random) phase  $\Delta \phi = (1/\hbar) \Delta \vec{p} \Delta \vec{x}$  with  $\Delta \vec{x} \propto 1/m$  the interferometer path separation. The effects of time imprecisions and Doppler shift induced imperfect population transfer is depicted in figure 10 (b). A deviation of the interferometer cycle times by  $\Delta T$  will lead to an additional momentum dependent phase term subject to thermal decoherence  $\phi_o = (\vec{p}/m) \vec{k} \Delta T = \vec{v} \vec{k} \Delta T = \vec{p}/\hbar \Delta \vec{x}$  with  $\vec{v} = \vec{p}/m$  the particle momentum, whose magnitude depends on the spatial wavepacket overlap. This defines a minimal required time precision that scales inversely with the particle mass. Similarly, a Doppler shift detuning  $\delta \sim \vec{v} \vec{k}$  will affect the population transfer of the interferometric beam splitter operations, an effect that is not removed by introducing decoupling sequences. Owing to the velocity variance mass scaling, its influence also decreases with increasing particle size. In a more general context, best seen in perturbative path integral approaches for the interferometer phase calculation [48], smaller space-time areas reduce the phase contributions of mass independent spatial Hamiltonian perturbations.

Note however that, despite the advantages outlined

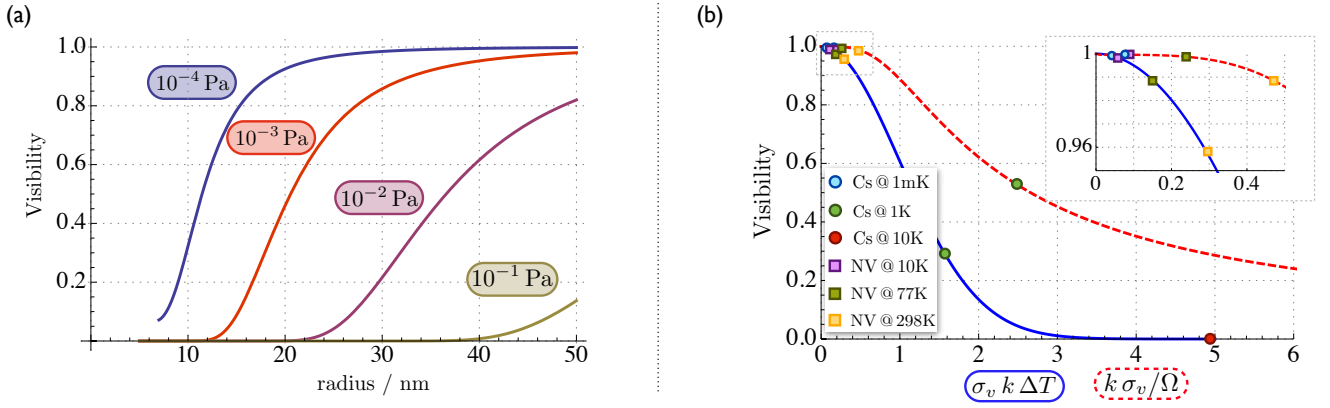


FIG. 10. **(a) Collisional decoherence:** Interferometer visibility for a (background gas) temperature of 10 K and different nanodiamond radii and pressures as indicated in the figure. The total interferometer time has been chosen as  $2T = 200 \mu s$  and the interferometric path splitting is assumed constant and approximated by its maximal value  $\Delta z = \hbar k^2 / m T$  with  $k = 2 \cdot 10^7 \text{ m}^{-1}$ . An isotropic elastic scattering cross section has been assumed in a description as developed in [47]. **(b) Time and pulse errors:** Visibility reduction for time (blue solid, open interferometer) and pulse errors (red dashed), arising from Doppler shift detunings, for different thermal velocity variances  $\sigma_v$ . Values for Cs atom and nanodiamond (radius 5 nm) setups at different temperatures are indicated in the figure, assuming  $\Omega = 2\pi \cdot 10 \text{ MHz}$  and  $\Delta T = 10 \text{ ns}$ , respectively.

above, from a practical perspective the interference with nanoparticles is much more complex compared to atomic setups (see also section II). In addition this decoherence scaling only holds for nanoparticles, because going to larger sizes would lead to significant other decoherence contributions like photon scattering and thermal decoherence [23] and would eventually end up in classical behaviour.

## VII. CONCLUSION

In this paper we have shown how interferometry with massive particles, with the specific examples of nanodiamonds, can improve existing bounds on proposed quantum gravity corrections to the energy dispersion relation. Assuming the Planck scale as the relevant scale for quantum gravity, this would even allow for an existence proof of the linear correction contribution under experimentally realistic parameters. However, despite its rather large proposed magnitude under optimal conditions, gravitation and a thermal distribution of momenta will in general render its observation inaccessible, which necessitates a revision of previously estimated bounds. As the requirements on the particle temperature and gravitation in a standard setup turn out to be quite challenging, we have proposed an alternative noise insensitive scheme based on an initial momentum transfer combined with a momentum inversion by gravitation. Last, the combination of the interferometric setup with decoupling sequences and mass scalings for decoherence and visibility reducing processes have been analyzed. The latter reveal an increasing robustness with the particle size, originating in decreasing spatial areas for increasing masses. This behaviour renders the interference of nanoparticles,

despite technical challenges, a viable scenario.

## ACKNOWLEDGMENTS

This work was supported by the Alexander von Humboldt Foundation, the EU STREP project EQuaM and the EU Integrating project SIQS.

- 
- [1] Hagar, A. *Discrete or Continuous? The Quest for Fundamental Length in Modern Physics* (Cambridge University Press, 2014).
- [2] Hossenfelder, S. Minimal length scale scenarios for quantum gravity. *Living Rev. Relativity* **16** (2013).
- [3] Giddings, S. B. Is string theory a theory of quantum gravity? *Found. Phys.* **43**, 115–139 (2013).
- [4] Blau, M. & Theisen, S. String theory as a theory of quantum gravity: a status report. *Gen. Relativ. Gravit.* **41**, 743–755 (2009).
- [5] Ashtekar, A. & Lewandowski, J. Background independent quantum gravity: a status report. *Class. Quantum Grav.* **21**, R53 (2004).
- [6] Magueijo, J. & Smolin, L. Lorentz invariance with an invariant energy scale. *Phys. Rev. Lett.* **88**, 190403 (2002).
- [7] Amelino-Camelia, G. Relativity in spacetimes with short-distance structure governed by an observer-independent (Planckian) length scale. *Int. J. Mod. Phys. D* **11**, 35–59 (2002).
- [8] Maggiore, M. A generalized uncertainty principle in quantum gravity. *Phys. Lett. B* **304**, 65–69 (1993).
- [9] Amelino-Camelia, G., Laemmerzahl, C., Mercati, F. & Tino, G. M. Constraining the energy-momentum dispersion relation with Planck-scale sensitivity using cold atoms. *Phys. Rev. Lett.* **103**, 171302 (2009).
- [10] Das, S. & Vagenas, E. C. Universality of quantum gravity corrections. *Phys. Rev. Lett.* **101**, 221301 (2008).
- [11] Ali, A. F., Das, S. & Vagenas, E. C. Proposal for testing quantum gravity in the lab. *Phys. Rev. D* **84**, 044013 (2011).
- [12] Pikovski, I., Vanner, M. R., Aspelmeyer, M., Kim, M. & Brukner, Č. Probing Planck-scale physics with quantum optics. *Nature Phys.* **8**, 393–397 (2012).
- [13] Mercati, F., Mazón, D., Amelino-Camelia, G., Carmona, J. M., Cortés, J. L., Induráin, J., Lämmerzahl, C. & Tino, G. M. Probing the quantum-gravity realm with slow atoms. *Class. Quantum Grav.* **27**, 215003 (2010).
- [14] Hogan, C. J. Interferometers as probes of Planckian quantum geometry. *Phys. Rev. D* **85**, 064007 (2012).
- [15] Berchera, I. R., Degiovanni, I., Olivares, S. & Genovese, M. Quantum light in coupled interferometers for quantum gravity tests. *Phys. Rev. Lett.* **110**, 213601 (2013).
- [16] Bekenstein, J. D. Is a tabletop search for Planck scale signals feasible? *Phys. Rev. D* **86**, 124040 (2012).
- [17] Chu, S. Atom interferometry. In Kaiser, R., Westbrook, C. & David, F. (eds.) *Coherent atomic matter waves*, vol. 72 of *Les Houches - Ecole d'Ete de Physique Theorique*, 317–370 (Springer, 2001).
- [18] Kasevich, M. & Chu, S. Atomic interferometry using stimulated Raman transitions. *Phys. Rev. Lett.* **67**, 181 (1991).
- [19] Kasevich, M. & Chu, S. Measurement of the gravitational acceleration of an atom with a light-pulse atom interferometer. *Appl. Phys. B* **54**, 321–332 (1992).
- [20] Wicht, A., Hensley, J. M., Sarajlic, E. & Chu, S. A preliminary measurement of the fine structure constant based on atom interferometry. *Phys. Scr.* **2002**, 82 (2002).
- [21] Bouchendira, R., Cladé, P., Guellati-Khélifa, S., Nez, F. & Biraben, F. New determination of the fine structure constant and test of the quantum electrodynamics. *Phys. Rev. Lett.* **106**, 080801 (2011).
- [22] Dimopoulos, S., Graham, P. W., Hogan, J. M., Kasevich, M. A. & Rajendran, S. Atomic gravitational wave interferometric sensor. *Phys. Rev. D* **78**, 122002 (2008).
- [23] Hornberger, K., Gerlich, S., Haslinger, P., Nimmrichter, S. & Arndt, M. Colloquium: quantum interference of clusters and molecules. *Rev. Mod. Phys.* **84**, 157 (2012).
- [24] Hackermüller, L., Hornberger, K., Brezger, B., Zeilinger, A. & Arndt, M. Decoherence of matter waves by thermal emission of radiation. *Nature* **427**, 711–714 (2004).
- [25] Aharonovich, I., Greentree, A. D. & Prawer, S. Diamond photonics. *Nature Photon.* **5**, 397–405 (2011).
- [26] Jelezko, F., Gaebel, T., Popa, I., Gruber, A. & Wrachtrup, J. Observation of coherent oscillations in a single electron spin. *Phys. Rev. Lett.* **92**, 076401 (2004).
- [27] Balasubramanian, G., Neumann, P., Twitchen, D., Markham, M., Kolesov, R., Mizuochi, N., Isoya, J., Achard, J., Beck, J., Tissler, J., Jacques, V., Hemmer, P. R., Jelezko, F. & Wrachtrup, J. Ultralong spin coherence time in isotopically engineered diamond. *Nature Mat.* **8**, 383–387 (2009).
- [28] De Lange, G., Wang, Z., Riste, D., Dobrovitski, V. & Hanson, R. Universal dynamical decoupling of a single solid-state spin from a spin bath. *Science* **330**, 60–63 (2010).
- Naydenov, B., Dolde, F., Hall, L. T., Shin, C., Fedder, H., Hollenberg, L. C., Jelezko, F. & Wrachtrup, J. Dynamical decoupling of a single-electron spin at room temperature. *Phys. Rev. B* **83**, 081201 (2011).
- Cai, J.-M., Naydenov, B., Pfeiffer, R., McGuinness, L. P., Jahnke, K. D., Jelezko, F., Plenio, M. B. & Retzker, A. Robust dynamical decoupling with concatenated continuous driving. *New J. Phys.* **14**, 113023 (2012).
- [29] Geiselmann, M., Juan, M. L., Renger, J., Say, J. M., Brown, L. J., de Abajo, F. J. G., Koppens, F. & Quidant, R. Three-dimensional optical manipulation of a single electron spin. *Nature Nanotech.* **8**, 175–179 (2013).
- [30] Neukirch, L. P., Gieseler, J., Quidant, R., Novotny, L. & Vamivakas, A. N. Observation of nitrogen vacancy photoluminescence from an optically levitated nanodiamond. *Opt. Lett.* **38**, 2976–2979 (2013).
- [31] Yale, C. G., Buckley, B. B., Christle, D. J., Burkard, G., Heremans, F. J., Bassett, L. C. & Awschalom, D. D. All-optical control of a solid-state spin using coherent dark states. *PNAS* **110**, 7595–7600 (2013).
- [32] Hilser, F. & Burkard, G. All-optical control of the spin state in the NV-center in diamond. *Phys. Rev. B* **86**, 125204 (2012).
- [33] Scala, M., Kim, M. S., Morley, G. W., Barker, P. F. & Bose, S. Matter-wave interferometry of a levitated thermal nano-oscillator induced and probed by a spin. *Phys. Rev. Lett.* **111**, 180403 (2013).
- [34] Schleich, W. P., Greenberger, D. M. & Rasel, E. M. A representation-free description of the Kasevich–Chu interferometer: a resolution of the redshift controversy. *New J. Phys.* **15**, 013007 (2013).
- [35] Alfaro, J., Morales-Tecotl, H. A. & Urrutia, L. F. Quantum gravity corrections to neutrino propagation. *Phys. Rev. Lett.* **84**, 2318 (2000).
- [36] Mattingly, D. Modern tests of Lorentz invariance. *Living Rev. Rel.* **8**, 2003 (2005).



- [37] Togan, E., Chu, Y., Imamoglu, A. & Lukin, M. Laser cooling and real-time measurement of the nuclear spin environment of a solid-state qubit. *Nature* **478**, 497–501 (2011).
- [38] Wieser, M. E. *et al.* Atomic weights of the elements 2011 (IUPAC technical report). *Pure Appl. Chem.* **85**, 1047–1078 (2013).
- [39] Hanneke, D., Fogwell, S. & Gabrielse, G. New measurement of the electron magnetic moment and the fine structure constant. *Phys. Rev. Lett.* **100**, 120801 (2008).
- [40] Aoyama, T., Hayakawa, M., Kinoshita, T. & Nio, M. Tenth-order QED contribution to the electron  $g-2$  and an improved value of the fine structure constant. *Phys. Rev. Lett.* **109**, 111807 (2012).
- [41] Chiow, S.-w., Herrmann, S., Chu, S. & Müller, H. Noise-immune conjugate large-area atom interferometers. *Phys. Rev. Lett.* **103**, 050402 (2009).
- [42] Chiow, S.-w., Kovachy, T., Chien, H.-C. & Kasevich, M. A. 102  $\hbar k$  large area atom interferometers. *Phys. Rev. Lett.* **107**, 130403 (2011).
- [43] Kiesel, N., Blaser, F., DeliĆ, U., Grass, D., Kaltenbaek, R. & Aspelmeyer, M. Cavity cooling of an optically levitated submicron particle. *PNAS* **110**, 14180–14185 (2013).
- [44] Amelino-Camelia, G., Freidel, L., Kowalski-Glikman, J. & Smolin, L. Relative locality and the soccer ball problem. *Phys. Rev. D* **84**, 087702 (2011).
- [45] Magueijo, J. Could quantum gravity phenomenology be tested with high intensity lasers? *Phys. Rev. D* **73**, 124020 (2006).
- [46] Hossenfelder, S. Multiparticle states in deformed special relativity. *Phys. Rev. D* **75**, 105005 (2007).
- [47] Hornberger, K. & Sipe, J. E. Collisional decoherence reexamined. *Phys. Rev. A* **68**, 012105 (2003).
- [48] Storey, P. & Cohen-Tannoudji, C. The Feynman path integral approach to atomic interferometry. A tutorial. *Journal de Physique II* **4**, 1999–2027 (1994).
- [49] Vacanti, G., Fazio, R., Kim, M., Palma, G., Paternostro, M. & Vedral, V. Geometric-phase backaction in a mesoscopic qubit-oscillator system. *Phys. Rev. A* **85**, 022129 (2012).
- [50] Cadoret, M., De Mirandes, E., Cladé, P., Nez, F., Julien, L., Biraben, F. & Guellati-Khélifa, S. Atom interferometry based on light pulses: Application to the high precision measurement of the ratio  $h/m$  and the determination of the fine structure constant. *Eur. Phys. J. Spec.* **172**, 121–136 (2009).

# Appendix A: Interferometer phase in the Ramsey Bordé setup

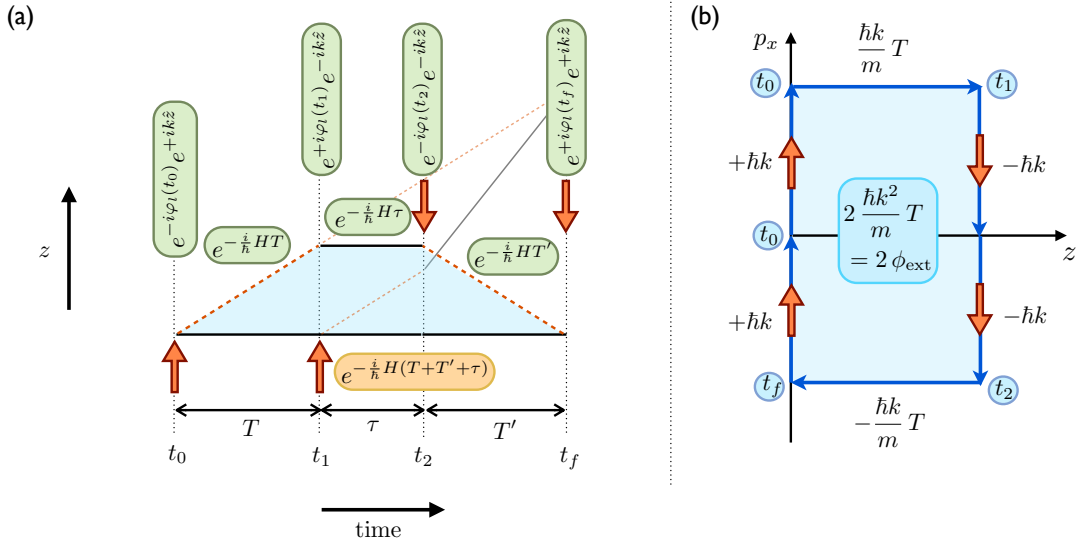


FIG. A1. **Ramsey Bordé interferometer and phase space area** (a) Ramsey Bordé interferometry setup. Black and red dashed lines correspond to the internal state  $|g\rangle$  and  $|e\rangle$ , respectively. Red arrows indicate  $\pi/2$ -laser pulses in the corresponding direction. The unitary evolution operators for the upper and lower path, leading to  $U^{(g)}$  as defined in the main text, are shown in green and orange boxes, respectively. (b) Phase space evolution and area for  $E(p) = p^2/(2m)$  in the absence of an external potential. Laser interaction paths are marked by the superimposed red arrow and in addition the corresponding times are given under the assumption of instantaneous laser pulses.

In here we will derive the interferometric phase of the Ramsey Bordé setup as depicted in figure A1(a) using the operator based formalism developed in [34]. Thereby we will focus on keeping the analysis as general as possible, what allows for a simple inclusion of modified energy dispersion relations or accelerating inertial forces at a later stage. In addition, based on the kinetic energy, we will give a general rule for the phase calculation in the specific case of at most an inertial force.

We will assume the two level system  $\{|g\rangle, |e\rangle\}$  initially prepared in the state  $|\psi_i\rangle = |g, p\rangle$ , with  $p$  describing the external, motional degrees of freedom. The  $\pi/2$ - laser interaction pulse, that takes the role of a beam-splitter, is described by the unitary operation

$$U_{\pi/2} = \frac{1}{\sqrt{2}} \left( \mathbb{1} - i \left[ e^{-i\varphi} e^{ik\hat{z}} \sigma_+ + e^{i\varphi} e^{-ik\hat{z}} \sigma_- \right] \right) \quad (\text{A.1})$$

with the rotation axis defined by  $\sigma_\varphi = \cos(\varphi) \sigma_x + \sin(\varphi) \sigma_y$ . Note that, most importantly, the recoil contribution  $\exp(ik\hat{z})$  leads to a splitting in momentum space, which is responsible for the relevant splitting in the external degrees of freedom (‘interferometric beam splitter operation’). During the free evolution periods, the external degrees of freedom evolve according to

$$U_f = \exp \left( -(i/\hbar) H(\hat{p}, \hat{z}) t \right) \quad \text{with} \quad H(\hat{p}, \hat{z}) = E(\hat{p}) + V(\hat{z}) \quad \text{and} \quad V'(\hat{z}) = \text{const.} \quad (\text{A.2})$$

Herein  $E(\hat{p})$  denotes the kinetic energy and  $V(\hat{z})$  an external potential; importantly we restricted this potential to inertial forces that are linear in position, as only in that case a simple closed form for the phase can be obtained. Note however that for the case of quadratic harmonic oscillator potentials, a straightforward phase expression can be obtained as well by a slightly different approach [33, 49]. The internal degrees of freedom evolution follows out of

$$U_{\text{in}} = \exp \left( -(i/\hbar) \int^t H_{\text{in}}(t') dt' \right) \quad \text{with} \quad H_{\text{in}} = -\hbar \delta(t)/2 \sigma_z \quad (\text{A.3})$$

in a frame rotating with the pulsed laser frequency,  $\delta(t)$  the corresponding detuning and  $\sigma_z$  the Pauli z-matrix defined in the two level internal state system. This term can be included conveniently in (A.1) by replacing  $\varphi \rightarrow \varphi_l(t) =$

$\varphi(t) + \int^t \delta(t') dt'$ . Right after the interferometer sequence, and restricting to the two paths involved in the sequence, i.e. the ones that lead to equal states, the system ends up in the state

$$|\psi_f\rangle = \left(\frac{1}{\sqrt{2}}\right)^4 \left( [U_u^{(g)} + U_l^{(g)}] |\psi_i\rangle + i [U_u^{(e)} - U_l^{(e)}] |\psi_i\rangle \right) \quad (\text{A.4})$$

with  $U_u$  and  $U_l$  describing the evolution operators of the upper and lower path, respectively, and the left part evolution ends up in the atomic state  $|g\rangle$ , whereas the right one ends up in  $|e\rangle$  as indicated by the unitary operator indices  $g$  and  $e$ , respectively.

The probability to find the system in the internal state  $|g\rangle$  (=the initial state) after the interferometer sequence follows out of (A.4) and is given by

$$p_g = \text{tr}(|g\rangle\langle g| \otimes \mathbb{1} |\psi_f\rangle\langle\psi_f|) = \frac{1}{8} \left[ 1 + \frac{1}{2} \left( \langle\psi_i| U_l^{(g)\dagger} U_u^{(g)} |\psi_i\rangle + \text{c.c.} \right) \right]. \quad (\text{A.5})$$

Thus it remains to calculate  $U_l^{(g)\dagger} U_u^{(g)}$ , a quantity that delivers a pure phase for the closed interferometer setup here, thus making it independent of the specific form of the initial state  $|\psi_i\rangle$ . Note that, as both paths do end up in the same state, both evolutions are formally equivalent up to an operator ordering, i.e. the non-commutativity of operators is responsible for the appearance of an interferometric phase.

For the calculation we will follow two approaches, a direct evaluation of free evolution sequences and laser pulse interactions and an evaluation in an interaction frame with respect to  $V(\hat{z})$ , this latter one allowing for a simple generalization of the phase calculation.

### Important operator relations

We will begin by providing several important relations, that are obtained by using the operator identity  $\exp(-\alpha\hat{A})\hat{B}\exp(\alpha\hat{A}) = \sum_{\nu=0}^{\infty} (-\alpha)^\nu / \nu! [\hat{A}, \hat{B}]_\nu$  with  $[\hat{A}, \hat{B}]_0 = \hat{B}$  and  $[\hat{A}, \hat{B}]_\nu = [\hat{A}, [\hat{A}, \hat{B}]_{\nu-1}]$ , along with  $[\hat{z}, \hat{p}] = i\hbar$  and the assumed linear potential property  $V'(\hat{z}) = \text{const.}$  Thus it follows that

$$e^{\pm ik\hat{z}} e^{-i/\hbar H(\hat{p}, \hat{z})t} e^{\mp ik\hat{z}} = e^{-i/\hbar [H(\hat{p}, \hat{z}) + \Delta E(\hat{p}, \mp \hbar k)]t} \quad \text{with} \quad \Delta E(\hat{p}, \pm \hbar k) = E(\hat{p} \pm \hbar k) - E(\hat{p}) \quad (\text{A.6})$$

and using that  $[p, V(\hat{z})] = V'(\hat{z}) [\hat{p}, \hat{z}]$

$$\Delta E_{\text{int}}^t(\hat{p}, \pm \hbar k) \equiv e^{i/\hbar H(\hat{p}, \hat{z})t} \Delta E(\hat{p}, \pm \hbar k) e^{-i/\hbar H(\hat{p}, \hat{z})t} = \Delta E(\hat{p} - V'(\hat{z})t, \pm \hbar k) \quad (\text{A.7})$$

where we would like to emphasize again that this simple form of (A.7) crucially relies on the fact that  $V'(\hat{z})$  is merely a c-number. Recalling the definition of the interaction picture in quantum mechanics, it then follows that

$$e^{i/\hbar H(\hat{p}, \hat{z})t} e^{-i/\hbar [H(\hat{p}, \hat{z}) + \Delta E(\hat{p}, \mp \hbar k)]t} = \exp\left(-i/\hbar \int_0^t \Delta E_{\text{int}}^{t'}(\hat{p}, \pm \hbar k) dt'\right) \quad (\text{A.8})$$

where the time ordering can be neglected as  $\Delta E_{\text{int}}^t$  depends exclusively on the operator  $\hat{p}$ .

### (i) Free evolution and pulses framework

In here we will evaluate the phase by analyzing the free evolution of the external degrees of freedom modified by the laser interactions at the specific times denoted in figure A1(a). Therefore the evolution operators take the form (with  $H \equiv H(\hat{p}, \hat{z})$ )

$$\begin{aligned} U_u^{(g)} &= e^{i\Delta\varphi} e^{ik\hat{z}} e^{-i/\hbar H(t_f - t_2)} e^{-ik\hat{z}} e^{-i/\hbar H(t_2 - t_1)} e^{-ik\hat{z}} e^{-i/\hbar H(t_1 - t_0)} e^{ik\hat{z}} \\ U_l^{(g)} &= e^{-i/\hbar H(t_f - t_0)} \end{aligned} \quad (\text{A.9})$$

with

$$\Delta\varphi = [\varphi_l(t_f) - \varphi_l(t_2) + \varphi_l(t_1) - \varphi_l(t_0)] = [\varphi(t_f) - \varphi(t_2) + \varphi(t_1) - \varphi(t_0)] + \int_{t_0}^{t_1} \delta(t') dt' + \int_{t_2}^{t_f} \delta(t') dt' \quad (\text{A.10})$$

that does take the value  $\Delta\varphi = 2\delta T$  for fixed laser phases and a constant detuning  $\delta(t) \equiv \delta$ . The basic idea for the simplification consists of bringing  $U_u^{(g)}$  to a form such that (A.8) can be applied; therefore using (A.6) and inserting identities one obtains

$$U_u^{(g)} = e^{i\Delta\varphi} \left[ e^{-i/\hbar HT'} e^{i/\hbar HT'} \right] e^{-i/\hbar [H + \Delta E(\hat{p}, -\hbar k)]T'} e^{-i/\hbar H\tau} \left[ e^{-i/\hbar HT} e^{i/\hbar HT} \right] e^{-i/\hbar [H + \Delta E(\hat{p}, \hbar k)]T}. \quad (\text{A.11})$$

Now using (A.8) and commuting  $\exp(-i/\hbar H\tau) \exp(-i/\hbar HT)$  to the left with the help of relation (A.7), one obtains

$$U_u^{(g)} = e^{i\Delta\varphi} e^{-i/\hbar H(T+T'+\tau)} \exp\left(-\frac{i}{\hbar} \int_0^T dt' [\Delta E(\hat{p} - V'(\hat{z})t', +\hbar k) + \Delta E([\hat{p} - V'(\hat{z})(T+\tau)] - V'(\hat{z})t', -\hbar k)]\right) \quad (\text{A.12})$$

in which the second  $\Delta E$  contribution can be interpreted as starting with the initial momentum  $\hat{p} = \hat{p} - V'(\hat{z})(T+\tau)$ , i.e. taking into account the acceleration influence up to the new ‘initial time’  $t_2$ .

Therefore the phase contribution follows as

$$\begin{aligned} U_l^{(g)\dagger} U_u^{(g)} &= e^{i\Delta\varphi} \exp\left(-\frac{i}{\hbar} \left[ \int_{t_0}^{t_1} \Delta E(\hat{p} - V'(\hat{z})t', +\hbar k) dt' + \int_{t_2}^{t_f} \Delta E(\hat{p} - V'(\hat{z})t', -\hbar k) dt' \right]\right) \\ &= e^{i\Delta\varphi} \exp\left(-\frac{i}{\hbar} \oint E[p(t')] dt'\right), \end{aligned} \quad (\text{A.13})$$

which simply corresponds to the kinetic energy integrated over the closed path (for  $T = T'$ ) and an additional internal phase contribution. As a remark, note that the derivation is much more simple in cases where there is no external potential present (or  $V(z) = \text{const.}$ ); in such a case it suffices to apply (A.6) to (A.10) and subsequently all exponents commute and can be added.

More generally we would like to point out that the phase of the motional degrees of freedom for any closed interferometer interacting with laser pulses and subject to at most inertial forces, corresponds just to the kinetic energy integrated along the path, i.e.  $\phi_{\text{ext}} = 1/\hbar \oint E[p(t')] dt'$ . This is intuitively to see in the interaction frame, for more complicated pulse sequences along with (A.6) and (A.7). Moreover it has been used previously for the phase evaluation, based on a semiclassical treatment, e.g. in [50].

### (ii) Interaction frame

The path evolution operators are most easily evaluated in an interaction frame with respect to the potential  $V(\hat{z})$ , in which case (A.7)  $H_{\text{int}} \equiv H_{\text{int}}(\hat{p}) = E(\hat{p} - V'(\hat{z})t)$  whereas the pulse components remain unchanged. Therefore

$$\begin{aligned} U_{u,\text{int}}^{(g)} &= e^{i\Delta\varphi} e^{ik\hat{z}} e^{-\frac{i}{\hbar} \int_{t_2}^{t_f} E(\hat{p} - V'(\hat{z})t') dt'} e^{-ik\hat{z}} e^{-\frac{i}{\hbar} \int_{t_1}^{t_2} E(\hat{p} - V'(\hat{z})t') dt'} e^{-ik\hat{z}} e^{-\frac{i}{\hbar} \int_{t_0}^{t_1} E(\hat{p} - V'(\hat{z})t') dt'} e^{ik\hat{z}} \\ U_{l,\text{int}}^{(g)} &= e^{-\frac{i}{\hbar} \int_{t_0}^{t_f} E(\hat{p} - V'(\hat{z})t') dt'}, \end{aligned} \quad (\text{A.14})$$

which do connect to (A.10) by  $U^{(g)} = \exp(-(i/\hbar)V(\hat{z})t_f)U_{\text{int}}^{(g)}$ . Now using that, in complete analogy to (A.6),  $\exp(\pm ik\hat{z}) \exp(\pm(i/\hbar) \int E(p, t') dt') \exp(\mp ik\hat{z}) = \exp(\pm(i/\hbar) \int E(p \pm \hbar k, t') dt')$ , the phase contribution can be straightforwardly evaluated to the form (A.13).

More generally we would like to point out that the phase of the motional degrees of freedom for any interferometer interacting with laser pulses, subject to at most inertial forces and closed in momentum space, corresponds just to the kinetic energy integrated along the path, i.e.  $\phi_{\text{ext}} = 1/\hbar \oint E[p(t')] dt'$ . This is intuitively to see in the interaction frame description. Moreover it has been used previously for the phase evaluation, based on a semiclassical treatment, e.g. in [50].

As an explicit example let us consider the standard energy dispersion relation  $E(\hat{p}) = \hat{p}^2/(2m)$ , a gravitational field  $V(\hat{z}) = m\vec{g}\vec{x}$  and assume that the laser phase is kept constant as well as the detuning. Noting that in the above derivation only the force component parallel to the pulse direction does contribute (the non-commuting  $\hat{p}$  and  $\hat{z}$  components), one obtains the well-known expression for the phase ( $T = T'$ )

$$\phi = \frac{\hbar k^2}{m} T + \vec{k} T \left[ \vec{g}(T + \tau) - \frac{1}{m} \Delta \vec{p}_{\text{acc}} \right] + 2\delta T \quad (\text{A.15})$$

where we introduced an additional acceleration of momentum  $\vec{p}_{\text{acc}}$  during the evolution time  $\tau$ , beside the gravitational influence, often used in experiments to increase the signal by adding a series of  $N$  acceleration pulses such that  $\Delta \vec{p}_{\text{acc}} = -N \hbar \vec{k}$ .



### 1. Relation to the phase space area

As previously noted by many authors, the motional part of the interferometer phase  $\phi_{\text{ext}}$  is, in many cases, related to the phase space area  $a_{\text{ps}}$  by the relation

$$a_{\text{ps}} = \oint p \, dz = 2 \phi_{\text{ext}}, \quad (\text{A.16})$$

which seems to hold for  $E(p) = p^2/(2m)$  by noting that in that case the phase space area (in the absence of any acceleration) is given by  $a_{\text{ps}} = 2(\hbar k^2)/mT$  (see figure A1(b)). Moreover such a relation can be strictly proven for trapped particle interferometers, in which the interferometer action can be described by a series of continuous displacements in phase space [49]; for the case considered here however, a description in terms of displacement operators seems inappropriate and a proof should involve the kinetic energy relation of the phase as has been shown in [34]

$$a_{\text{ps}} = \oint p \, dz = 2 \oint dt \frac{1}{2} m v^2 = 2 \oint dt E(p) = 2 \hbar \phi_{\text{ext}}. \quad (\text{A.17})$$

The relation to the kinetic energy follows exclusively for the standard dispersion relation  $E(p) = p^2/(2m)$ , whereas the last phase equation is just valid in case that the interferometric phase follows out of the relation  $\phi_{\text{ext}} = 1/\hbar \oint E[p(t')] \, dt'$ . Therefore the phase space relation according to (A.17) can just be guaranteed if two conditions are fulfilled: (i) the energy dispersion relation is of the standard form and (ii) the system is at most subject to inertial forces for the phase energy relation to be valid.

### Appendix B: The stability regime

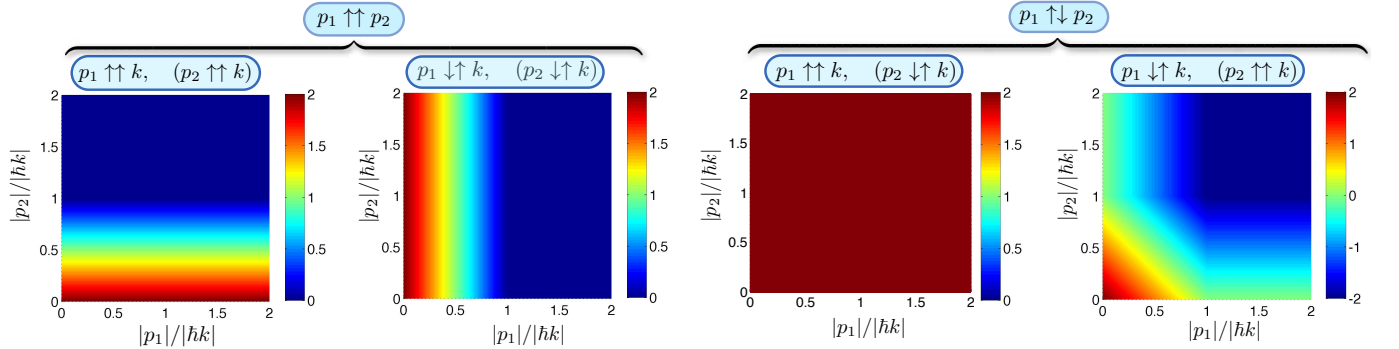


FIG. A2. **Phase contribution in the parallel regime.** Phase contribution  $\phi/(2\mu|\hbar k|T)$  vs different momentum values  $p_1$  and  $p_2$ . The third configuration corresponds to the stability regime.

In the absence of specifically designed momenta directions, the  $\xi_1$ -phase contribution is most likely to decay in the presence of momenta exceeding the beam splitter recoil contribution,  $|p| \geq |\hbar k|$ . As shown in section III, this leads to a suppression of coherent  $\xi_1$ -phase oscillations under the influence of gravitation and thermal momentum distributions. However based on an analysis in the regime  $|p| \gg |\hbar k|$  (5) it turned out that a change in the momentum with respect to the recoil direction in between the two interferometric cycles leads to a significant unsuppressed phase term, and more precise in a stability configuration  $\vec{p}_1^0 \uparrow\uparrow \vec{k} \ \&\& \ \vec{p}_2^0 \uparrow\downarrow \vec{k} (\Leftrightarrow \vec{p}_1^0 \uparrow\downarrow \vec{p}_2^0)$  the optimal phase  $\phi = 2\mu\hbar kT$  is recovered independently of the momentum value. Here, as already outlined in the main text, ‘parallel’ and ‘orthogonal’ refers to the direction of the momentum relative to the first recoil  $\vec{k}$  direction; the first interferometric cycle is defined by  $[t_0, t_1]$  and the second one by  $[t_2, t_f]$  (see figure 1). We will demonstrate here, that this does not only hold in the regime of large momenta, but in any possible limit as long as the parallel condition is fulfilled.

An orthogonal component will always lead to a decay with increasing momentum and that even holds for the individual cycles, i.e.  $p_1$  and  $p_2$  components alone. In contrast, for a parallel component only the combination of both will lead to a potential suppression. Figure A2 analyzes this effect in more detail for static, but potentially different parallel momenta  $p_1 = |\vec{p}_1^0|$ ,  $p_2 = |\vec{p}_2^0|$  for the two interferometer cycles. It turns out that, without a momentum direction change ( $\vec{p}_1 \uparrow\uparrow \vec{p}_2$ ), the phase contribution always decays to zero in the large momentum limit  $|p_1|, |p_2| \gg |\hbar k|$ ,

and therefore the only solution consists of working in the rather challenging  $|p_1|, |p_2| \ll |\hbar k|$  regime. In contrast, in a  $\vec{p}_1 \uparrow \downarrow \vec{p}_2$  configuration, i.e. if there occurs a change in the momentum direction, the large momentum limit is characterized by a non-zero, momentum independent phase. Particularly, the stability regime  $\vec{p}_1^0 \uparrow \uparrow \vec{k}$  &&  $\vec{p}_2^0 \uparrow \downarrow \vec{k}$  ( $\Leftrightarrow \vec{p}_1^0 \uparrow \downarrow \vec{p}_2^0$ ) retains this property in any possible momentum regime, as long as the parallel condition is fulfilled.

### Appendix C: Modified dispersion relation vs modified commutator relations

It is widely assumed that a quantization of space-time in quantum gravity will lead to a minimal length-scale of the order of the Planck length  $L_p = \hbar/(M_p c)$ , that can be accounted for by a modification of the commutator relation of the form [2]

$$[\hat{x}, \hat{p}] = C(\hat{p}) \quad (\text{A.1})$$

with  $C(\hat{p}) = i\hbar$  in the standard case of quantum mechanics and e.g.  $C(\hat{p}) = i\hbar(1 + \xi p^2/(M_p c)^2)$ , that will lead to a minimal lengthscale  $\Delta x = \sqrt{\xi} L_p$  according to the general uncertainty principle  $\Delta x \Delta p \geq -1/2 i \langle C(\hat{p}) \rangle$  [2, 11, 12]. Herein  $\xi$  denotes a dimensionless parameter that for a Planck-scale correction will be of order one and is in general upper bounded by the electroweak length scale to  $\xi \leq 10^{34}$  [10, 11]. Such a modified commutator relation will then lead to a modified interferometer phase, that can be calculated, at least in a perturbative way with respect to the Planck scale correction, in the formalism of Appendix A, and its measurement has already been proposed in a more simplistic setup in [12]. As the interferometer phase considered here corresponds merely to the kinetic energy integrated over a closed path, it is a natural question to ask if both, the modified energy dispersion relation and the modified commutator relation, are equivalent. That is, can the modified energy dispersion be reproduced by choosing the standard dispersion  $E(\hat{p}) = \hat{p}^2/(2m)$  and modifying the commutator instead (in particular with respect to (A.6) and its appearance in the phase (A.10))? For this purpose we will begin by defining the energy dispersion relation via the displacement operation as

$$E(\tilde{p}) = \left\langle p=0 \left| e^{-\frac{i}{\hbar} \tilde{p} \hat{x}} \frac{\hat{p}^2}{2m} e^{\frac{i}{\hbar} \tilde{p} \hat{x}} \right| p=0 \right\rangle \quad (\text{A.2})$$

that can be evaluated (see also Appendix A and using that  $[x, f(\hat{p})] = f'(\hat{p})[x, p]$ ) to

$$E(\tilde{p}) = \left\langle p=0 \left| \frac{1}{2m} \left[ \hat{p}^2 - 2\frac{i}{\hbar} \tilde{p} \hat{p} C(\hat{p}) - \frac{\tilde{p}^2}{\hbar^2} C(\hat{p})^2 + i\frac{\tilde{p}^3}{\hbar^3} C'(\hat{p}) C(\hat{p})^2 + \mathcal{O}(\tilde{p}^4) \right] \right| p=0 \right\rangle \quad (\text{A.3})$$

which corresponds to an expansion in the Planck scale correction. For the modification of the commutator relation given above, this would lead to (with  $\beta = \xi/(M_p c)^2$ )

$$E(\tilde{p}) = \frac{1}{2m} \left( \tilde{p}^2 + \frac{2}{3} \beta \tilde{p}^4 + \frac{17}{45} \beta^2 \tilde{p}^6 + \mathcal{O}(\beta^3) \right). \quad (\text{A.4})$$

It is worth to note that, due to the quadratic form of the unmodified energy dispersion relation, a correction term linear in the momentum does not appear according to (A.2), whereas the absence of higher order odd powers in (A.3) is only due to the specific form chosen for the commutator and in contrast to the absence of a linear term non-fundamental. Thus a quadratic correction could be reproduced by a modified commutator whereas a linear correction term is impossible within that framework. As a remark, such a conclusion is only valid if  $\hat{p}$  corresponds to the physical momentum; if in contrast  $\hat{p}$  is a function of the physical momentum operator as often used in quantum gravity approaches [2], a linear term correction would not be forbidden any more however related to a different coordinate framework of quantum mechanics.